JPEDAV (2005) 26:520-528
DOI: 10.1361/154770305X66664
1547-7037/$19.00 ©ASM International

Kinetics of Microstructure Evolution during Gaseous Thermochemical Surface Treatment

Marcel A.J. Somers and Thomas Christiansen

(Submitted July 12, 2005)

The incorporation of nitrogen or carbon in steel is widely applied to provide major improvements in materials performance with respect to fatigue, wear, tribology, and atmospheric corrosion. These improvements rely on a modification of the surface-adjacent region of the material by the (internal) precipitation of alloying element nitrides/carbides or by the development of a continuous layer of iron-based (carbo-) nitrides. The evolution of the microstructure during thermochemical treatments is not only determined by solid-state diffusion, but in many cases also by the kinetics of the surface reactions and the interplay with mechanical stress. In the present article a few examples, covering research on the interaction of carbon and/or nitrogen with iron-based metals, are included to illustrate the various aspects of gas-metal interactions.

1. Introduction

Gaseous thermochemical surface treatments such as nitriding and nitrocarburizing belong to the most versatile surface engineering processes of steels and allow improvement of the performance of components with respect to fatigue, wear, and atmospheric corrosion. In principle, during treatment the case developing can be subdivided into a surface layer consisting of compounds such as nitrides and carbonitrides with a diffusion zone underneath, containing alloying element (carbo)nitrides or a supersaturated interstitial solution of nitrogen in a metallic matrix. In the present article the various aspects of the kinetics of microstructure evolution during gas-solid interactions during thermochemical treatment are discussed. These aspects involve the implication of the competition between surface reaction kinetics and solid-state diffusion on nucleation of a compound at a surface and compound layer growth, the competition between carbon and nitrogen uptake during nitrocarburizing, and the modeling aspects of the growth of expanded austenite during nitriding of austenitic stainless steel.

The gas-solid interactions[1] to be discussed are essentially simple and concern nitriding in NH_3/H_2 and nitrocarburizing in $NH_3/CO_2/H_2$. In all cases atmospheric pressure applies. Dissociation reactions at the surface provide the atomic species adsorbed at the surface, which subsequently may be incorporated into the solid state or leave the surface again. For nitriding in NH_3/H_2, adsorbed nitrogen atoms can diffuse into the solid phase ϕ,

$$NH_3 \leftrightarrow N_{ad} + \frac{3}{2} H_2 \qquad \text{(Reaction Ia)}$$

$$N_{ad} \leftrightarrow [N]_\phi \qquad \text{(Reaction Ib)}$$

or, upon development of molecular nitrogen, leave the surface:

$$N_{ad} + N_{ad} \leftrightarrow N_2 \qquad \text{(Reaction Ic)}$$

For nitrocarburizing, a competition between a carburizing and a nitriding reaction occurs. Because of the presence of hydrogen, carburizing according to the following scheme is kinetically preferred.

$$CO_2 + H_2 \leftrightarrow CO + H_2O \qquad \text{(Reaction IIa)}$$

$$CO + H_2 \leftrightarrow C_{ad} + H_2O \qquad \text{(Reaction IIb)}$$

$$C_{ad} \leftrightarrow [C]_\phi \qquad \text{(Reaction IIc)}$$

2. Nucleation of Iron Nitride at an Iron Surface during Nitriding[2]

On gaseous nitriding of iron the first phase developing at the surface is γ'-Fe_4N_{1-x}, which nucleates upon exceeding the maximum solubility of nitrogen in iron in the region adjacent to the surface. The incubation time for the nucleation of γ' nitride depends on the competition between the flux of nitrogen atoms arriving at the surface and the flux of those leaving the surface. The flux of arriving nitrogen atoms is controlled by ammonia dissociation (reaction Ia); the fluxes of nitrogen atoms leaving the surface are the result of the development and desorption of N_2 (reaction Ic) and diffusion of nitrogen atoms into the solid state (reaction Ib). For an iron plate of infinite length and width with finite

This article is a revised version of the paper printed in the *Proceedings of the First International Conference on Diffusion in Solids and Liquids—DSL-2005*, Aveiro, Portugal, July 6-8, 2005, Andreas Öchsner, José Grácio and Frédéric Barlat, eds., University of Aveiro, 2005.

Marcel A.J. Somers and **Thomas Christiansen,** Department of Manufacturing Engineering, and Management, Technical University of Denmark, DK-2800 Kgs. Lyngby, Denmark. Contact e-mail: somers@ipl.dtu.dk.

thickness (L) and a uniform, initial nitrogen distribution (C_0), the fluxes of nitrogen atoms associated with the dissociation reaction of ammonia at the surface, J_{diss}, the desorption of molecular nitrogen from the surface, J_{des}, and solid-state diffusion into the substrate, J_{diff}, are given by Eq 1 to 3[2,3]:

$$J_{diss} = k \cdot (C_{eq} - C_S) \quad \text{(Eq 1)}$$

$$J_{des} = -k_2 \cdot \frac{K_S \cdot C_S^2}{1 + K_S \cdot C_S} \quad \text{(Eq 2)}$$

$$J_{diff} = J|_{z=0} = -D_N^{\alpha} \left.\frac{\partial C_N}{\partial z}\right|_{z=0} \quad \text{(Eq 3)}$$

where k is the reaction rate constant for ammonia dissociation, C_{eq} is the nitrogen concentration in α-iron for equilibrium with the gas phase, C_S is the actual concentration of nitrogen in the solid state adjacent to the surface, k_2 is a rate constant of the formation of molecular nitrogen, K_S is the equilibrium constant of segregation of nitrogen atoms at the iron surface, and $z = 0$ indicates the position of the surface. To obtain the nitrogen depth distribution as a function of nitriding time, Fick's second law:

$$\frac{\partial C_N}{\partial t} = D_N^{\alpha} \frac{\partial^2 C_N}{\partial z^2} \quad \text{(Eq 4)}$$

has to be solved for the set of boundary conditions given by Eq 1 to 3. At the time where the surface concentration C_S exceeds the solubility limit for nitrogen in α-Fe a driving force for the nucleation of γ'-Fe_4N_{1-x} is established. This nitriding time is taken as the incubation time for iron nitride nucleation. In Fig. 1(a) the incubation time thus calculated is given as a function of the nitriding potential,[1] K_N, for nitriding temperatures ranging from 743 to 863 K (details of the calculations and the data used are given in Ref 2 and 3). Evidently, the incubation time decreases with increasing nitriding potential. It follows from Fig. 1(a) that the formation of N_2 only affects the calculated incubation time for nitriding potentials just beyond the critical nitriding potential where ferrite can be stable. The effect of N_2 formation is a prolongation of the incubation period by maximally 10% (at 863 K) and decreases dramatically with decreasing temperature. The experimental investigation of the development of iron nitrides at a ferrite surface was carried out with light microscopy of the polished as-nitrided surface. Identification of the nitride phases was done with x-ray diffraction analysis.

The development of nitrides on grain surfaces rather than at grain boundaries (cf. Fig. 1b) was taken as a criterion for successful nucleation because the calculations do not take

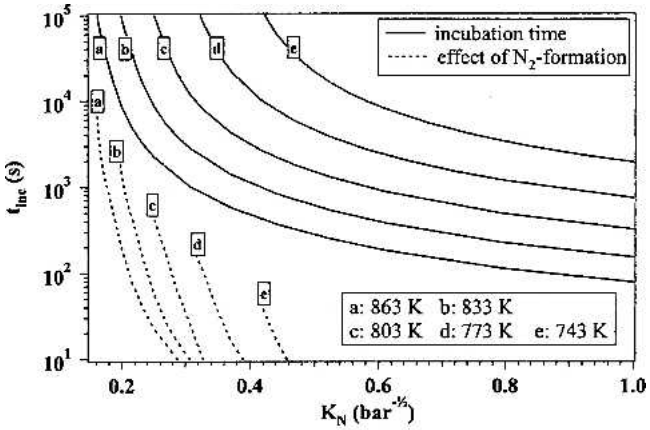

(a)

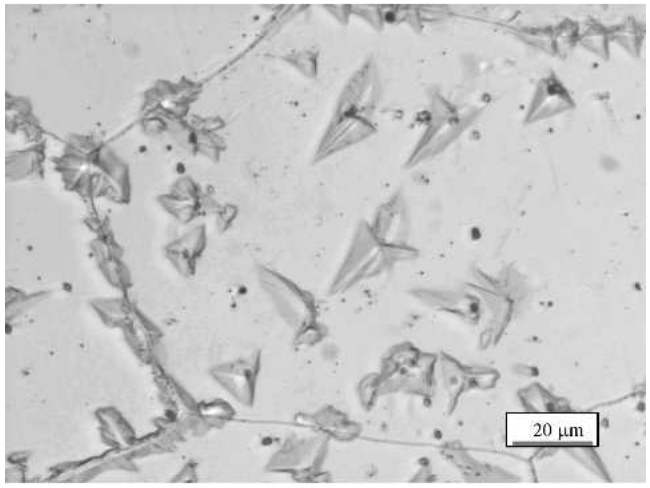

(b)

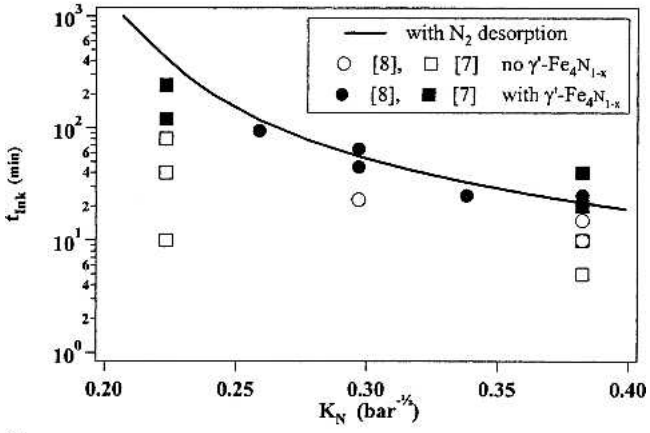

(c)

Fig. 1 (a) Calculated incubation time for establishing a driving force for the nucleation of γ'-Fe_4N_{1-x} on pure iron. The dashed curves represent the additional incubation time caused by N_2 development at the surface. (b) Light microscopy of polished surface H_2-reduced and nitrided. Nitriding was performed at 833 K at nitriding potential $K_N = 0.38$ bar$^{-1/2}$ ($= 1.2\ 10^{-3}$ Pa$^{-1/2}$) for 20 min. (c) Comparison of experimental and calculated incubation times at 833 K

[1]Nitriding potential is proportional to the nitrogen activity in the solid state for equilibrium with the gas phase,

$$K_N = \frac{p_{NH_3}}{p_{H_2}^{3/2}}$$

the occurrence of grain boundaries into account. The experimental incubation times for γ'-Fe_4N_{1-x} nucleation are generally shorter than the times calculated for attaining the maximum lattice solubility of nitrogen in ferrite, i.e., establishing a driving force for nitride nucleation (Fig. 1c). These systematic differences are attributed to differences in the surface conditions (composition and topography) of the samples used in the present experiments and those used in the experiments from which the rates of the surface reactions were assessed.[2]

3. Nitride Layer Growth under Combined Surface Reaction and Diffusion Control[4]

On nitriding, the growth kinetics of the compound layer during nitriding is usually assumed to be controlled by solid-state diffusion of nitrogen through the phases constituting the compound layer; the diffusion of iron atoms can be neglected.[5] The growth of γ'-Fe_4N_{1-x} monolayers or the ε-Fe_2N_{1-z}/γ'-Fe_4N_{1-x} double layers on ferrite can be evaluated from considering the fluxes entering and leaving the sublayers (for mathematical descriptions, see Ref 5). The assumptions, usually made to arrive at a mathematical description of the growth kinetics, involve local equilibrium at the solid/solid interfaces as well as at the surface. It can be assumed that the composition in each of the sublayers changes linearly with depth, provided that the composition-dependent diffusion coefficients D_N^φ are replaced by the composition-weighted (effective) diffusion coefficient, $\langle D_N^\varphi \rangle$, for each of the sublayers[5]:

$$\langle D_N^\phi \rangle = \int_{y_{N,\varphi}^{min}}^{y_{N,\varphi}^{max}} (D_N^\phi)^* \cdot \frac{d \ln a_N}{d \ln C_N} \cdot dy_{N,\varphi} \qquad \text{(Eq 5)}$$

with

$$(D_N^\varphi)^* = RT(1 - y_{N,\varphi})M_N^\varphi \qquad \text{(Eq 6)}$$

where $(D_N^\varphi)^*$ is the tracer diffusion coefficient of nitrogen in phase φ, $y_{N,\varphi}^{min}$ and $y_{N,\varphi}^{min}$ are the minimum and maximum occupancies of the interstitial sublattice in phase φ, and $M_{N,\varphi}^{max}$ is the mobility of nitrogen atoms in phase φ. The thermodynamic factor $d \ln a_N / d \ln C_N$ in Eq 4, where a_N is the activity of nitrogen and C_N the concentration of nitrogen, follows directly from the thermodynamics of the phases involved (cf. Ref 5 to 7 and references therein). For ε/γ' double layers the assumption of local equilibrium at the gas/solid interface is clearly in conflict with experimental findings (cf. Fig. 2 and Ref 2, 7); local equilibrium at the solid/solid interfaces appears to be in good agreement with experimental results. Generally, the nitrogen content in the ε phase close to the surface is significantly lower than the content corresponding to local equilibrium with an imposed nitrogen activity. This lower nitrogen content is attributed to the competition between the relatively slow kinetics of ammonia dissociation, the desorption of molecular nitrogen gas from the surface, and solid-state diffusion into ε nitride.

A model assuming local equilibrium at the solid/solid interfaces in the compound layer and a dynamic situation at the gas/solid interface is presented in Fig. 3. Analogous to the case of nucleation, the dynamic situation at the surface is described by Eq 1 to 3. The equations describing double layer growth under the condition of no local equilibrium at the surface have been published elsewhere.[8]

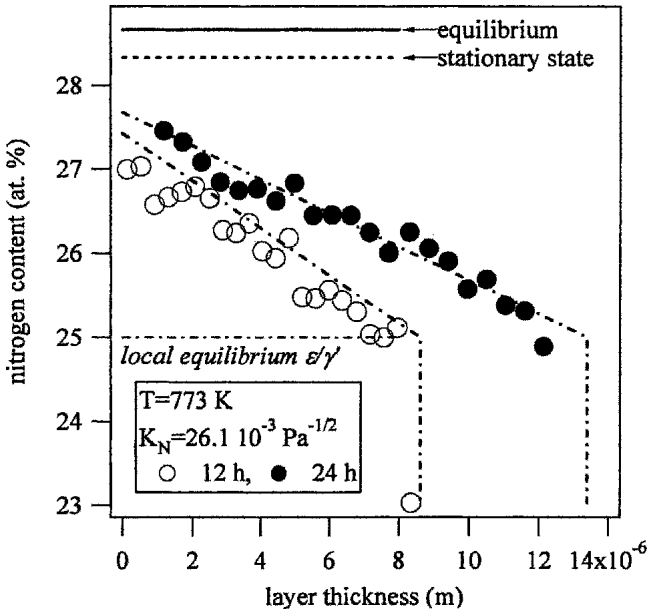

Fig. 2 Comparison of experimental and modeled nitrogen profiles for a dynamic state at the surface[4,7]

The evolution of the layer thicknesses of ε phase and γ'-nitride were described mathematically by the model in Fig. 3 under the above conditions, adopting k, k_2, K_S for ε phase and $(D_N^{\gamma'})^*$ and M_N^ε as fit parameters. Layer growth kinetics at 773 K at a relatively high nitriding potential is shown in Fig. 4. The dashed lines represent the simulated layer growth kinetics if the model from Ref 5 is adopted, which presumes local equilibrium at all interfaces, including the surface, and only one fit parameter ($\langle D_N^\varepsilon \rangle$ or M_N^ε). The model in Fig. 3 provides a better description of the evolution of the layer thickness than the model presuming local equilibrium at the surface (Fig. 4) and, perhaps more convincingly, the evolution of the nitrogen depth profile (Fig. 2).

The major discrepancy between the modeled and experimental data in Fig. 4 concerns the thickness of the γ' layer for relatively short nitriding times. Further improvement of describing the evolution of this part would involve incorporation of the nucleation of the γ' layer at the surface, which was left out of the present model to keep the number of fitting parameters as low as possible. Furthermore, it was found that upon exceeding the maximum solubility of nitrogen in ferrite, the γ'-layer does not form instantaneously as a layer, but by nucleation and subsequent coalescence (cf. Ref 2, 5) and references therein). As a consequence nitrogen incorporation can occur through both ferrite and the γ' nuclei, resulting in a thicker γ' layer than would be obtainable for diffusion through a γ' layer only (as reflected by the experimental data in Fig. 4). Another issue that deserves

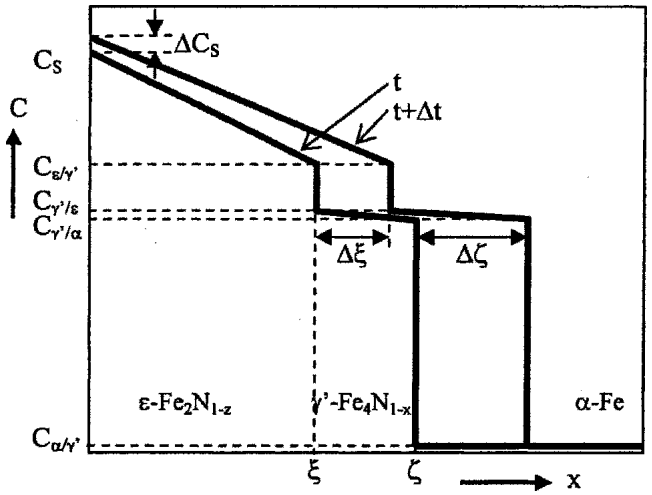

Fig. 3 Model for double layer growth. Local equilibrium prevails at all solid/solid phase boundaries. For a time increment *dt* the sublayers increase in thickness by dξ and dζ, whereas the surface concentration increases by ΔC_S. Linear concentration profiles are assumed in the sublayers.

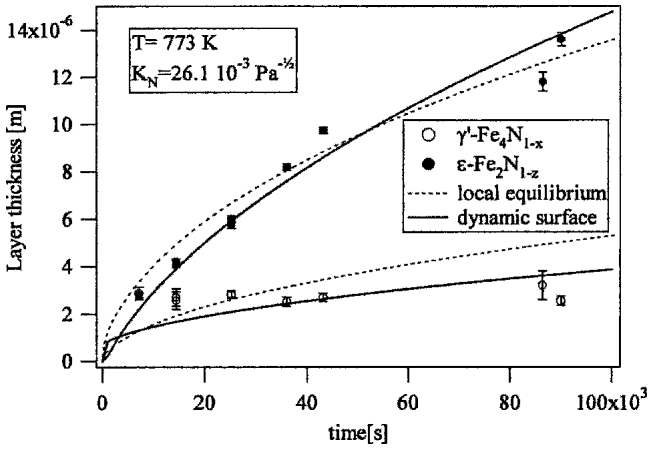

Fig. 4 Results of modeling double layer growth for the cases of local equilibrium (dashed lines) and a dynamic state (solid lines) at the surface

future attention is the occurrence of compositionally induced compressive stress profiles in the two nitride layers (cf. Ref 9 and references therein). This topic will be discussed in section 7.

4. Microstructural Evolution of the Compound Layer during Nitrocarburizing[10]

On gaseous *nitrocarburizing* the nucleation of the phases constituting the compound layer depends on the competition of the surface reactions I and II. The carburizing reaction proceeds much faster than the nitriding reaction. Hence, the carbon solubility in the substrate is exceeded earlier than the nitrogen solubility, and carbide or a carbonitride would be expected to nucleate. The nucleation of γ′ iron nitride is suppressed because of the low solubility of carbon in this

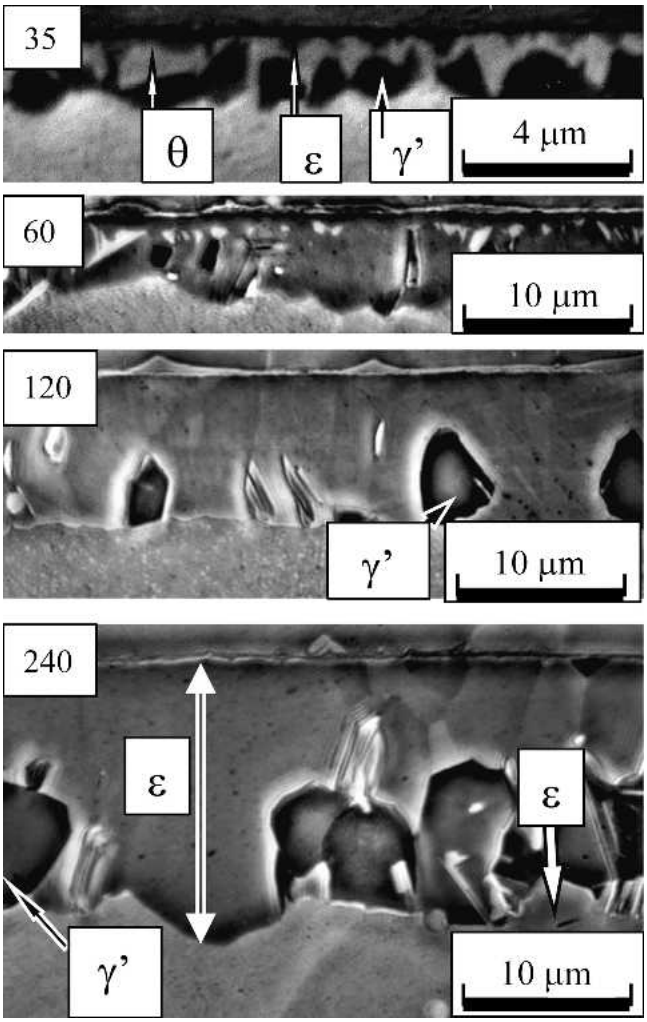

Fig. 5 Light microscopy of polished surfaces H_2-reduced and nitrided. Nitriding was performed at 833 K at nitriding potential $K_N = 0.38$ bar$^{-1/2}$ ($= 1.2\ 10^{-3}$ Pa$^{-1/2}$) for 15 min.

phase. On nitrocarburizing pure iron the first phase appearing at the surface was observed to be cementite (θ-Fe_3C) for various combinations of nitriding and carburizing activities.[10] A first appearance of the carbonitride phase ε-$Fe_2(N,C)_{1-z}$ in the compound layer was observed to be promoted by a high nitriding potential and to be retarded by a high carburizing activity, but was never observed to nucleate as the first phase.

In the sequel the microstructural evolution of the compound layer is discussed for the following combination of nitrogen and carbon activities: $a_N = 753$; $a_C = 1.37$. The morphological and compositional evolution of the compound layer on iron during nitrocarburizing under these conditions is presented in Fig. 5. After the initial development of cementite, the ε phase becomes dominant in the compound layer on prolonged treatment. The content of cementite decreases and, eventually, becomes zero. Concurrently, the amount of γ′ phase increases (Fig. 5), particularly in the part of the compound layer adjacent to the substrate. The evolution of the composition depth profiles shows that the nitrogen content at the surface increases with

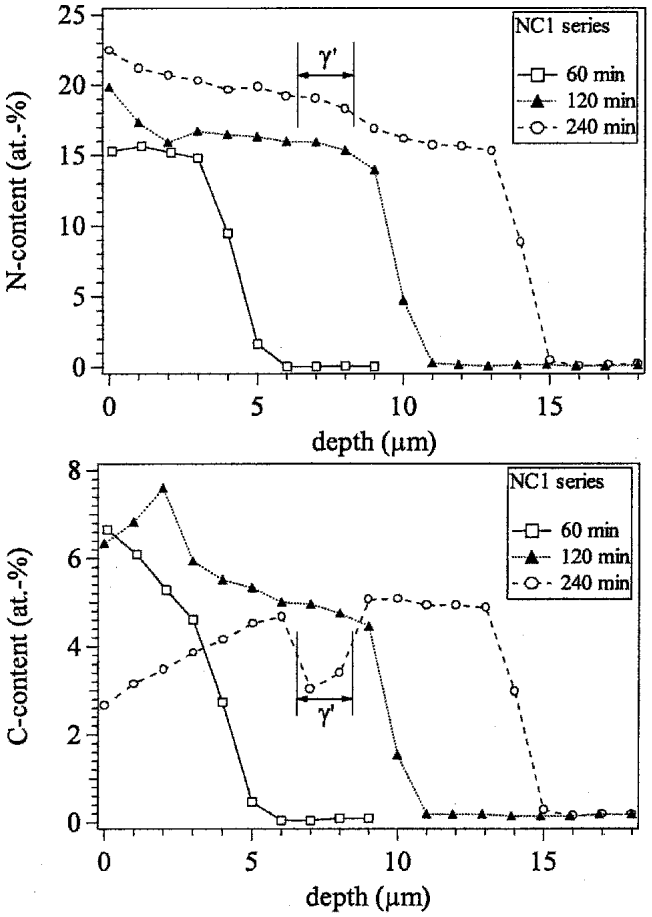

Fig. 6 EPMA nitrogen and carbon depth profiles determined on cross sections of the samples in Fig. 5 for 60, 120, and 240 min

time, whereas the carbon content at the surface decreases complementarily (Fig. 6). This relatively slow increase of the nitrogen content is consistent with the observation of a continuously increasing nitrogen content in ε phase on nitriding because of the relatively slow kinetics of ammonia dissociation at (and nitrogen desorption from) the iron surface, which allowed an initially strong absorption of carbon. Needless to say, modeling of the microstructure evolution of the compound layer during nitrocarburizing is currently not possible because it involves nucleation and dissolution of phases as well as composition changes. Most parameters necessary for such modeling are (as yet) quantitatively undetermined.

A very first attempt to model the growth kinetics of the compound layer during nitrocarburizing for a simple phase constitution of the compound layer and local equilibrium at the surface and solid/solid interfaces is presented in Ref 11.

5. Dissolution of Nitrogen in Austenitic (fcc) Stainless Steel[12,13]

A very recent development in the thermochemical treatment of iron-based materials is nitriding of stainless steel,

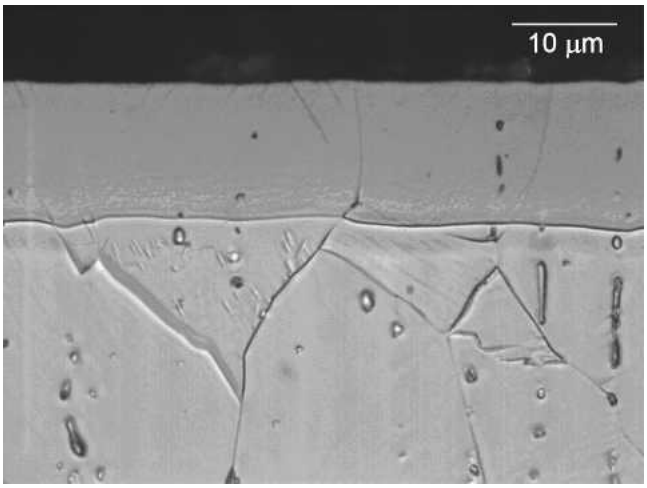

Fig. 7 Layer of expanded austenite obtained by nitriding stainless steel (AISI 316) at 718 K for 22 h in 60% NH_3/40% H_2 (Ref 12, 13)

with the purpose of improving the surface wear performance without impairing the excellent corrosion properties. This can only be achieved when the hardening process does not hinder chromium atoms from forming the self-repairing chromium-based oxide layer that provides corrosion resistance. Because chromium has a relatively strong affinity for forming nitrides, the temperature should be low to prevent chromium atoms from diffusing to nucleation sites for chromium nitrides (surface, grain boundaries, dislocations). Accordingly, a metastable equilibrium between nitrogen in the gas phase and nitrogen in the solid state can be achieved, so-called expanded austenite (or S phase), where nitrogen is interstitially dissolved in the strongly oversaturated fcc lattice. The nitrogen occupancy of the interstitial fcc lattice can be as high as $y_N = 0.61$, which is higher than the nitrogen contents hitherto reported to be achievable for iron nitrides under gaseous nitriding conditions. In micrographs expanded austenite is typically recognized as a featureless surface layer (cf. Fig. 7) with a high hardness.

The nitrogen contents dissolvable in (stress-free) expanded austenite are colossal and can be controlled by adjusting the nitrogen activity in the gas phase (Fig. 8a). Experimentally the data in Fig. 8(a) were obtained thermogravimetrically by nitriding of thin coupons (5-7.5 μm) in pure NH_3 and thereafter equilibrating the coupons in a NH_3/H_2 mixture with known nitrogen activity a_N; the lowest a_N was obtained in pure H_2.

The lattice expansion associated with interstitial dissolution of nitrogen in the austenite lattice (Fig. 8b) implies the occurrence of large stresses and steep stress gradients over a growing layer of expanded austenite. Compressive stresses of the order of several GPa and stress gradients of the order of a 10^{15} Pa·m^{-1} are no exception.[12,13] Consequently, the assessment of nitrogen diffusion coefficients from layer-growth kinetics experiments can only lead to stress-affected diffusion coefficients without general validity. Another complication in the determination of diffusion coefficients of nitrogen from the evolution of the nitrogen

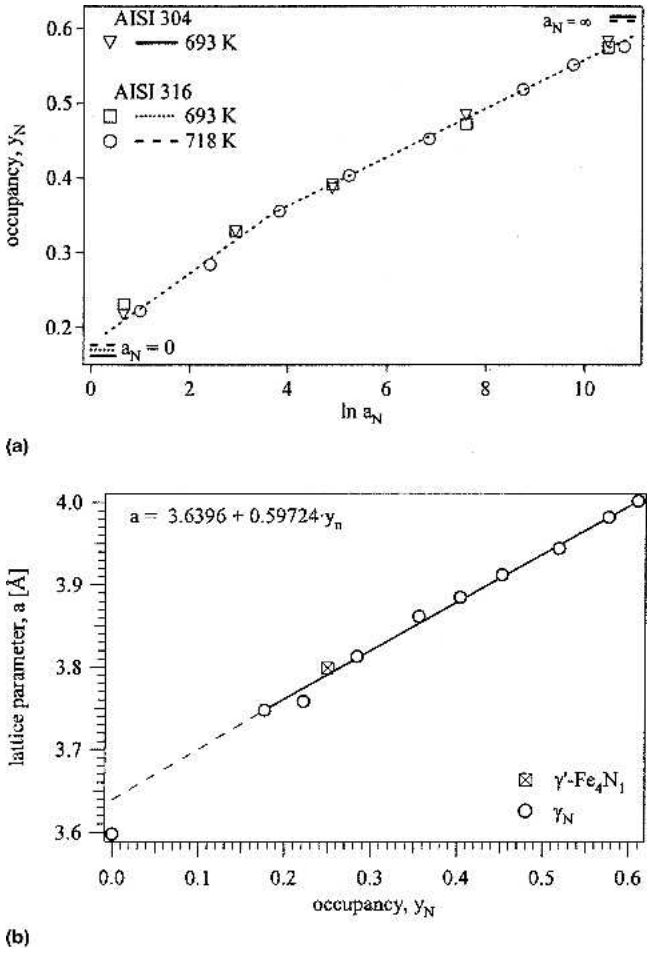

Fig. 8 (a) Nitrogen occupancy, y_N, of the interstitial fcc lattice of expanded austenite as a function of the imposed nitrogen activity, a_N, in the NH_3/H_2 gas mixture. (b) Lattice parameter of expanded austenite vs occupancy of the interstitial fcc lattice

concentration profile is the occurrence of trapped nitrogen in expanded austenite. As shown in Fig. 8(a) the nitrogen occupancy of the interstitial lattice obtained for $a_N = 0$ leaves a nitrogen content conforming to $y_N = 0.17$ in the sample, which corresponds to the chromium content. This strongly suggests that a nitrogen content corresponding to Cr:N = 1:1 is strongly bound in the sample. To be able to distinguish between the diffusion of strongly bound and less strongly bound nitrogen atoms the following method was applied for the determination of the concentration-dependent diffusion coefficient of nitrogen in expanded austenite.

As mentioned above, thin coupons were nitrided in a thermobalance for continuous monitoring of the change of the sample weight and thus the nitrogen content. After equilibrating in pure NH_3, the samples were equilibrated at a slightly lower a_N, by adjusting the composition of the NH_3/H_2 gas mixture. Consequently, the sample weight decreases by denitriding until a new stationary state (metastable equilibrium) between gas and sample is attained. The kinetics of weight decrease was described mathematically with the equation for desorption from a plate, taking the

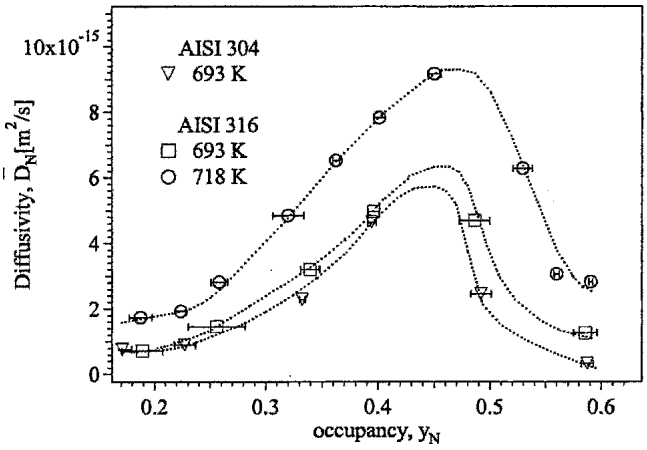

Fig. 9 Effective diffusion coefficients of nitrogen in expanded austenite (both AISI 304 and 316) vs nitrogen occupancy of the interstitial fcc lattice

diffusivity as a constant fitting parameter. By repeating this procedure for a range of a_N values, a range of effective values for the diffusion coefficients in the composition ranges for the actual denitriding steps is obtained. The influence of stress (gradients) on these values is considered small.

The effective diffusivities thus obtained are depicted in Fig. 9. Evidently, the diffusion coefficient of nitrogen in expanded austenite is concentration dependent and has a maximum value for nitrogen occupancies of about $y_N = 0.45$. Qualitatively, these results can be reasoned as follows. The expansion of the austenite lattice by dissolution of nitrogen is likely to facilitate the transfer of a nitrogen atom from an octahedral interstitial site of the fcc lattice to a tetrahedral site, which can be considered the activated state for interstitial diffusion in fcc lattices. Thus, the activation energy for the diffusion of nitrogen is reduced. With increasing nitrogen content the occupancy of the interstitial lattice increases, which reduces the probability that a nitrogen atom in the activated state can jump to an unoccupied octahedral site. Consequently, the diffusion coefficient is reduced. Evidently, for nitrogen contents exceeding $y_N = 0.45$ the latter reduced probability for diffusion outweighs the reduced activation energy.

5.1 Calculation of Nitrogen Profiles in Nitrided Austenite

On the basis of the composition-dependent diffusivity of nitrogen in expanded austenite it is possible to estimate the evolution of the nitrogen concentration profile as a function of the nitriding parameters temperature, gas composition, and time. In the modeling of nitrogen diffusion in expanded austenite it is assumed that nitrogen up to $y_N = 0.17$ is immobile and does not contribute to long-range diffusion (cf. Fig. 8a). A similar assumption was recently done for modeling the diffusion of nitrogen in ferritic iron-chromium alloys,[14,15] where distinction was made between so-called mobile and immobile excess nitrogen atoms[15]: all nitrogen atoms, including excess nitrogen, dissolved in the expanded ferrite lattice were considered mobile and contributed

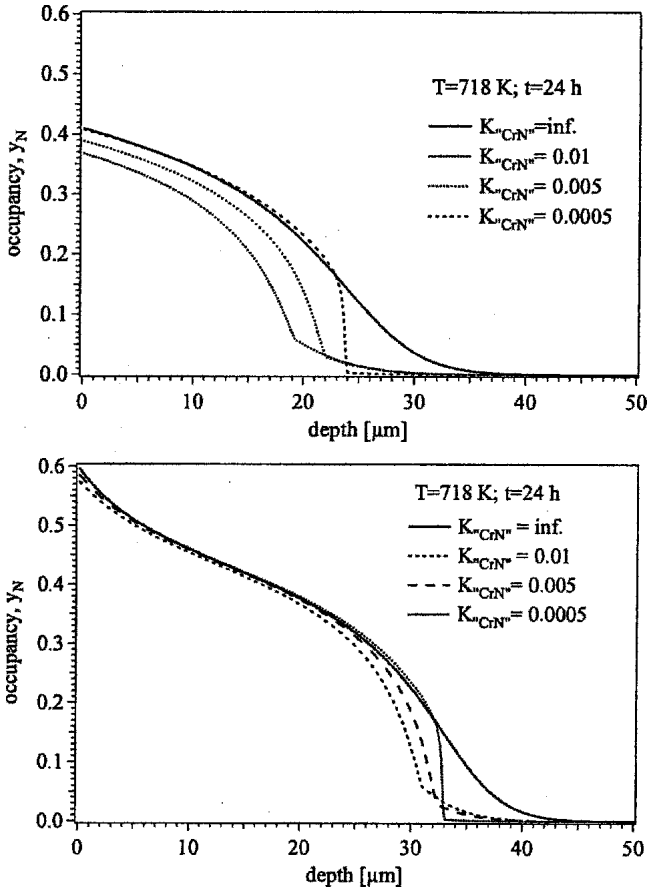

Fig. 10 Calculated nitrogen depth profiles in stainless steel AISI 316 after nitriding at 718 K for 24 h at a nitriding potential K_N = 1.39 $bar^{-1/2}$ (top) and 595 $bar^{-1/2}$ (bottom). Various values of the solubility product $K_{"CrN"}$ were chosen.

(solely) to the development of the nitrogen concentration profile, whereas (excess) nitrogen atoms residing in CrN and at the interface between CrN platelets and ferrite were considered immobile. In the present case of nitrogen in expanded austenite all nitrogen atoms are in solid solution, but evidently the chemical environments are different.

The first results of our calculations, with a model similar to that in Ref 14 and 15, but with a concentration-dependent nitrogen diffusion coefficient (Fig. 9) and immobile nitrogen considered as nitrogen trapped by chromium atoms (not as nitrides!) in the expanded austenite lattice are given in Fig. 10. The solubility product, $K_{"CrN"} = y_{Cr}.y_N$, of chromium and nitrogen in the austenitic lattice, i.e., the combination of chromium and nitrogen contents below which no trapping occurs, is not known for the present temperature. Therefore various values were considered in our calculations. The solubility product, $K_{"CrN"}$ effectively governs the trapping behavior of nitrogen. For a $K_{"CrN"}$ value of nil, infinitely strong trapping of nitrogen at the trap sites occurs. Conversely, an infinitely high value of $K_{"CrN"}$ implies that trapping does not occur at all.

The calculated profiles show a striking qualitative resemblance to those presented in the literature and are in qualitative agreement with the observation of a thin diffusion zone in front of the expanded austenite layer (cf. Fig. 7). Further refinement of the model appears necessary because the effects of compositionally-induced stresses as well as the effect of the kinetics of the surface reaction(s) were omitted in the present modeling. Furthermore, the diffusivity of nitrogen for compositions conforming to $y_N < 0.17$ is not known and was estimated by an extrapolation of diffusivities determined at higher nitrogen contents (Fig. 9).

5.2 Residual Stress in Expanded Austenite Layers

Stress-depth distributions over expanded austenite layers were determined with x-ray diffraction analysis and successive removal of very thin sublayers. It was recognized that the simultaneous occurrence of a stress-depth profile and a composition profile demands unraveling of the influences of stress (lattice strain) and composition on the lattice spacing and can lead to the occurrence of ghost stresses after data evaluation.[16] For the present case of residual stress in expanded austenite the ghost stresses can easily exceed 1 GPa.[17] Depth profiles of the strain-free lattice spacing in expanded austenite (which is directly proportional to the interstitial atom content) and residual stress are given in Fig. 11 for two expanded austenite layers obtained by nitriding or carburizing. Compressive stresses were obtained in all investigated samples.[12,13] Typically, the compressive stresses in γ_N and γ_C layers are of the order of several GPa, up to 7-8 GPa compression in γ_N layers. The very high compressive stresses are caused by the compositionally induced expansion of the austenite lattice (cf. Fig. 8b). However, the residual stress values expected from pure elastic accommodation of the expanded austenite lattice, as reflected by the strain-free lattice parameter (Fig. 11b), are twice as high. This discrepancy can be explained by an anticipated change of the elastic constants with interstitial atom content (which was not taken into account) and the occurrence of plastic deformation in the layers during growth. Evidently, the part of the lattice expansion which is accommodated elastically in the γ_N layer shown in Fig. 11 changes close to the surface because the (elastic) stress value decreases toward the surface, whereas the lattice expansion caused by the nitrogen content has its maximum value at the surface. This is explained from pushing individual grains out of the surface and possibly local crack formation.

6. Interaction of Stress and Kinetics of Microstructure Evolution

Qualitatively, the occurrence of compositionally induced stresses in the growing layers has the following implications for the layer growth kinetics:

- A situation of local equilibrium at the surface is no longer given by absorption isotherms as determined for homogeneous stress-free samples (cf. Ref 5, 6, and Fig. 8a) but should also take elastic strain energy into account.[18] For the present case of compressive stresses at the surface, this leads to lower nitrogen contents than reflected by the current (stress-free) thermodynamic data.

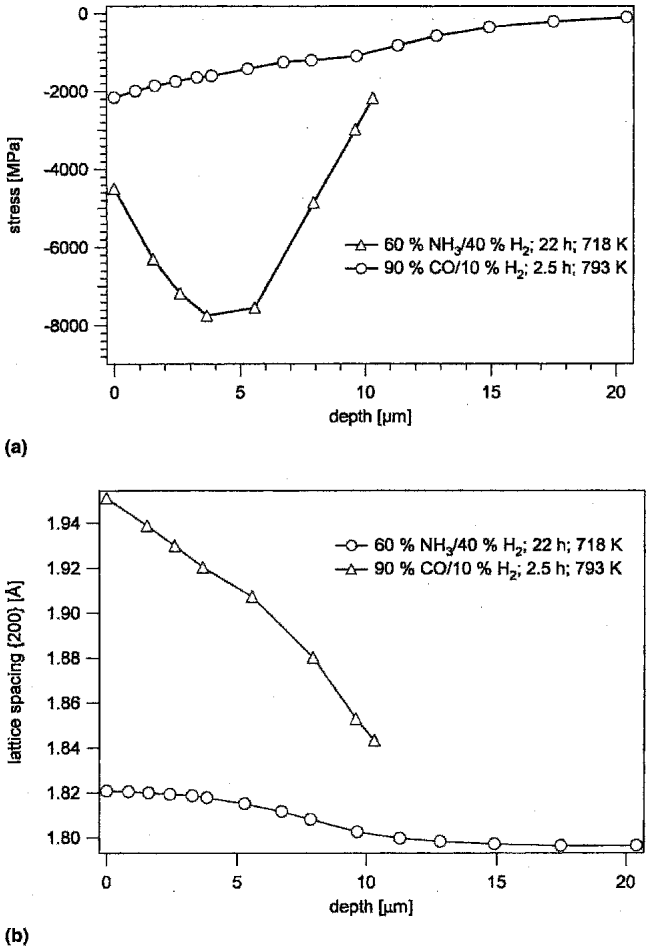

Fig. 11 (a) Residual stress and (b) strain-free lattice spacing profiles for γ_N and γ_C layers obtained under the nitriding and carburizing conditions as given in the legend. Stress and lattice spacing were obtained by x-ray diffraction.

- A compressive stress has a pressure effect on the diffusion coefficient.[19] In principle, this implies that the effective diffusivities/mobilities obtained as fit parameters in Section 3 (Fig. 4) are affected by this pressure effect and have no general validity.
- A stress gradient, such that the maximum compressive stress occurs at the surface, provides an extra driving force for nitrogen atoms to diffuse to larger depth. This also implies that effective diffusivities/mobilities obtained from fitting layer thickness data are affected by the compositionally induced stresses.

For the present cases of nitrogen and carbon diffusion in iron-based interstitial systems the effects of compositionally induced stress appear to be of considerable importance, most specifically for the case of expanded austenite where exorbitantly high compressive stresses of 7-8 GPa were found (Fig. 11 and Ref 12, 13). For the present interstitial systems the strategy to be followed for quantifying the effect of stress on diffusion and vice versa is combining experiments on thin foils, for determining the stress-unaffected diffusion coefficients as a function of composition. Thereafter, the kinetics of the incorporation of nitrogen (or carbon) into bulk samples, as studied by weight gain (in situ), layer growth kinetics, and evolution of the composition profile can be compared with the predictions on the basis of the stress-unaffected thermodynamics and diffusion parameters as well as with a model that incorporates the stress and the kinetics of surface reaction(s).

7. Conclusions

The kinetics of gas-metal interactions in iron-based interstitial systems is not controlled exclusively by solid-state diffusion of the interstitial elements as might be expected at first consideration. It was demonstrated for the case of nitriding of iron that the kinetics of surface reactions can have a strong influence too. In the case of nitrocarburizing a competition between nitriding and carburizing is initially (kinetically) won by carburizing, but on prolonged time the nitriding reaction dominates thermodynamically. The case of the growth of expanded austenite in austenitic stainless steel was addressed. In all evaluations up until now the role of compositionally induced residual stresses on the description of the thermodynamics and the diffusion coefficients was omitted. Nevertheless, compositionally induced stress values of several GPa can result for interstitial systems, as shown for nitrogen and carbon in expanded austenite. Future research should focus on the role of stress on diffusion.

References

1. H.J. Grabke, Kinetics of Gas-Solid Interactions, *Mater. Sci. Forum,* Vol 154, 1994, p 69-85
2. P.B. Friehling, F.W. Poulsen, and M.A.J. Somers, Nucleation of Iron Nitrides During Gaseous Nitriding of Iron; the Effect of a Preoxidation Treatment, *Z. Metallkde.,* Vol 92, 2001, p 589-595
3. H.C.F. Rozendaal, E.J. Mittemeijer, P.F Colijn, and P.J van der Schaaf, The Development of Nitrogen Concentration Profiles on Nitriding Iron, *Metall. Trans. A,* Vol 14, 1983, p 395-399
4. M.A.J. Somers and P.B. Friehling, Modellierung der Keimbildungs- und Wachs-tumskinetik der Verbindungsschicht beim Nitrieren von Reineisen, *Härterei-Tech. Mitt.,* Vol 57, 2002, p 415-420 (in German)
5. M.A.J. Somers and E.J. Mittemeijer, Layer-Growth Kinetics on Gaseous Nitriding; Evaluation of Diffusion Coefficients for Nitrogen in Iron-Nitrides, *Metall. Mater. Trans. A,* Vol 26, 1995, p 57-74
6. M.A.J. Somers, Thermodynamics, Kinetics, and Microstructural Evolution of the Compound Layer; a Comparison of the States of Knowledge of Nitriding and Nitrocarburising, *Heat Treat. of Met.,* Vol 27, 2000, p 92-102
7. E.J. Mittemeijer and M.A.J. Somers, Thermodynamics, Kinetics and Process Control of Nitriding, *Surf. Eng.,* Vol 13, 1997, p 483-497
8. P.B. Friehling, Nucleation and Growth of the Compound Layer During Gaseous Nitriding of Iron; the Effect of Preoxidation, Ph.D. Thesis, Technical University of Denmark, 2000
9. M.A.J. Somers, Modeling Nitriding of Iron; from Thermody-

namics to Residual Stress, *J. Phys. IV France,* Vol 120, 2004, p 21-33
10. H. Du, M.A.J. Somers, and J. Ågren, Microstructural and Compositional Evolution of Compound Layers during Gaseous Nitrocarburising, *Metall. Mater. Trans. A,* Vol 31, 2000, p 195-211
11. H. Du and J. Ågren, Theoretical Treatment of Nitriding and Nitrocarburizing of Iron, *Metall. Mater. Trans. A,* Vol 27, 1996, p 1073-1080
12. T. Christiansen and M.A.J. Somers, Randschichthärtung von rostfreiem Stahl durch Gasnitrieren und Gascarburieren bei niedrigen Temperaturen, *Härtereí-Tech. Mitt.,* Vol 60, 2005, p 207-214 (in German)
13. T. Christiansen, Low Temperature Surface Hardening of Stainless Steel, Ph.D. Thesis, Technical University of Denmark, 2004
14. Y. Sun and T. Bell, A Numerical Model of Plasma Nitriding of Low Alloy Steels, *Mater. Sci Eng. A,* Vol 224, 1997, p 33-47
15. R. Schacherl, P.C.J. Graat, and E.J. Mittemeijer, The Nitriding Kinetics of Iron-Chromium Alloys: The Role of Excess Nitrogen, Experiments, and Modeling, *Metall. Mater. Trans. A,* Vol 35, 2004, p 3387-3398
16. M.A.J. Somers and E.J. Mittemeijer, Development and Relaxation of Stress in Surface Layers; Composition and Residual Profiles in γ'-Fe_4N_{1-x} Layers on α-Fe Substrates, *Metall. Trans. A,* Vol 21, 1990, p 189-204
17. T. Christiansen and M.A.J. Somers, Reconstruction of Stress and Composition Profiles from X-Ray Diffraction Experiments—How to Avoid Ghost Stresses, *Mater. Sci. Forum,* Vol 443-444, 2004, p 91-94
18. J.C.M. Li, Physical Chemistry of Some Microstructural Phenomena, *Metall. Trans. A,* Vol 9, 1978, p 1353-1380
19. D.L. Beke, I.A. Szabó, Z. Erdélyi, and G. Opposits, Diffusion-Induced Stresses and Their Relaxation, *Mater. Sci. Eng. A,* Vol 387-389, 2004, p 4-10